INTERNATIONAL JOURNAL OF
RADIATION ONCOLOGY • BIOLOGY • PHYSICS
www.redjournal.org

BIOLOGY CONTRIBUTION

A Novel Focal Duodenal Radiation Injury Model Reveals Dose-, Time-, and Spatially Dependent Microbiome Perturbations After Radiation Injury

LeMoyne Habimana-Griffin, MD, PhD,[a,b] Jerome Prusa, PhD,[b,c] Bin Wang, MS,[b,c] Lori Strong, RT,[a] Jie Ning, MS,[b,c] Erick S. Ramirez Tovar, BS,[b,c] Kelsey Toth, PhD,[d] Blake Butler, BA,[b,c] Francisco J. Reynoso, PhD,[e] Stephanie Markovina, MD, PhD,[a] Matthew A. Ciorba, MD,[f] and Gautam Dantas, PhD[b,c,g,h,i]

[a]*Department of Radiation Oncology, Washington University School of Medicine in St. Louis, St. Louis, Missouri;* [b]*The Edison Family Center for Genome Sciences and Systems Biology, Washington University School of Medicine, St. Louis, Missouri;* [c]*Department of Pathology and Immunology, Division of Laboratory and Genomic Medicine, Washington University School of Medicine, St. Louis, Missouri;* [d]*Division of Oncology, Department of Medicine, Washington University School of Medicine in St. Louis, St. Louis, Missouri;* [e]*Medical Affairs, Varian, a Siemens Healthineers Company, Palo Alto, California;* [f]*Division of Gastroenterology, Department of Medicine, Washington University School of Medicine in St. Louis, St. Louis, Missouri;* [g]*Department of Molecular Microbiology, Washington University School of Medicine, St. Louis, Missouri;* [h]*Department of Biomedical Engineering, Washington University in St. Louis, St. Louis, Missouri; and* [i]*Department of Pediatrics, Washington University School of Medicine, St. Louis, Missouri*

Received Apr 7, 2025; Revised Oct 1, 2025; Accepted for publication Nov 4, 2025

Purpose: The duodenum is a key organ at risk during sterotactic ablative radiotherapy (SABR). Understanding mechanisms of radiation-induced intestinal injury (RIII) could reveal novel strategies to reduce SABR toxicities. The gut microbiome contributes to RIII; however, existing preclinical models either require surgical manipulation or fail to recapitulate high-dose conformal treatment fields used during SABR, confounding microbiome studies. We developed a noninvasive focal bowel irradiation model to assess microbiome dynamics in both the duodenum and the stool after high-dose duodenal irradiation.

Corresponding author: Gautam Dantas, PhD; E-mail: dantas@wustl.edu

Author Responsible for Statistical Analysis: LeMoyne Habimana-Griffin was responsible for the statistical analyses.

Disclosures: M.A.C. receives consulting fees from Janssen Pharmaceuticals, Pfizer, AbbVie, and Geneoscopy.

M.A.C. serves on data safety monitoring or advisory boards for Janssen Pharmaceuticals, Pfizer, AbbVie, and Geneoscopy. M.A.C. declares sponsored research support from Incyte, Pfizer, and Janssen Pharmaceuticals. S. M. is the PI of an ongoing clinical trial sponsored by GlaskoSmithKline. L. H.G. was supported by RSNA Research Resident Grant #RR2336. J.P. was supported by the National Cancer Institute of the National Institutes for Health (T32CA113275 and P30CA091842). The rest of the authors declare no conflicts of interest.

Data Sharing Statement: To facilitate transparency, reproducibility, and enable subsequent investigations building on this work, the code used for data analysis in this study will be made publicly available on GitHub https://github.com/dantaslab/2025_DuodenumRTMicrobiome on acceptance of the manuscript. In addition, the sequencing data will be deposited in the NCBI Sequence Read Archive (BioProject ID: PRJNA1365926). Additional information necessary to reproduce this work is available from the corresponding author on request.

Acknowledgments—We thank Skye Fishbein and Bejan Mahmud for conversations motivating this work. We thank Skye Fishbein for her guidance in designing microbiome studies. We thank Carmen Bergom for her comments and constructive feedback on the draft manuscript. We thank Kymberli May, Malick Ndao, Phillip Tarr, and the Digestive Disease Research Core Center at Washington University (NIDDK P30 DK052574) for assistance with histology and digitization of slides. We thank Eric Martin, Brian Koebbe, Jessica Hoisington-Lopez, and MariaLynn Crosby of the Edison Family Center for Genome Sciences and Systems Biology for sequencing expertise and computational support. We thank Julie Prior, Erin Teubner, Rui Tang, Mikhail Berezin, Monica Shokeen, and the Molecular Imaging Center at Washington University (NIH - S10OD027042, NIH - S10OD025264, NCI P30 CA091842) for discussions and support of imaging experiments.

Supplementary material associated with this article can be found in the online version at doi:10.1016/j.ijrobp.2025.11.011.

Int J Radiation Oncol Biol Phys, Vol. 125, No. 2, pp. 590–602, 2026

https://doi.org/10.1016/j.ijrobp.2025.11.011

Methods and Materials: C57BL/6J mice received sham treatment or focal irradiation (12 or 18 Gy) to the proximal duodenum using a small animal irradiator. Stool and duodenal tissue samples were collected at days 4, 14, and 91 after treatment and processed for bacterial 16S rRNA gene V4 region amplicon sequencing (Illumina MiSeq platform). Microbiome diversity metrics were calculated, and multivariable linear mixed modeling identified bacterial taxa associated with radiation therapy.
Results: Oral iodine contrast enabled duodenum visualization, and 100% of mice survived until euthanasia. Focal duodenal irradiation led to dose- and time-dependent changes in duodenal bacterial community composition that were not observed in stool. At days 4 and 14 after treatment, 18 duodenal taxonomic groups were significantly perturbed, whereas only 2 taxa were significantly altered in the stool.
Conclusions: Our focal duodenal irradiation model is safe, well tolerated, and easy to implement. It enables characterization of microbiome perturbations during both the acute and late phases of injury and serves as a platform for testing new RIII mitigation strategies. Our findings reveal that irradiation-induced changes in the duodenal microbiome are dose-, time-, and spatially dependent and are not reflected in stool samples. These results underscore the imperative of directly assessing tissue-associated microbiota, as relying solely on stool samples risks overlooking critical, localized microbial dynamics that may drive injury and repair.

Introduction

The duodenum is essential for digestion and nutrient absorption. The duodenum and proximal jejunum uniquely absorb iron and calcium, neutralize acidic chyme from the stomach, and deliver pancreatic enzymes and bile to facilitate digestion.[1] The duodenum is vulnerable during radiation therapy, and duodenal dose constraints can limit effective treatment of abdominal tumors.[2] Understanding mechanisms of duodenal radiotoxicity may yield strategies to mitigate the side effects of treatment and increase the therapeutic ratio of abdominal radiation therapy.

Preclinical data suggest that the gut microbiome modulates radiation-induced intestinal injury (RIII).[3] The microbiologically sterile gut of a germ-free mouse is protective of RIII from total body irradiation (TBI).[4] Similarly, antibiotic treatment can abrogate RIII after abdominal radiation.[5] In contrast, preclinical[6,7] and translational studies[8] have identified commensal and probiotic microbes that mitigate gastrointestinal injury from TBI or whole abdominal irradiation (WAI). These findings have led to clinical trials investigating orally administered probiotics as a potential treatment to reduce the severity of RIII-associated diarrhea, showing promising results.[9] Collectively, these findings indicate that bacteria of the gut microbiome play a complex and multifaceted role in RIII and underscore the need to distinguish beneficial and detrimental bacterial taxa impacting RIII.

Most existing preclinical models of RIII use TBI or WBI,[10] which do not reflect the dose distributions used in abdominopelvic radiation for patients with cancer.[11] A notable exception is a contribution by Gerassy-Vainberg et al,[12] who examined microbiome perturbations in colon tissue and stool in a murine radiation proctitis model using brachytherapy to focally injure the rectum. They found that focal irradiation of the rectum induced microbiome perturbations in both stool and damaged tissues. Furthermore, transferring stool from irradiated mice to germ-free mice increased susceptibility to radiation- or chemically induced colitis compared with stool from unirradiated mice, suggesting that irradiation-induced microbiome disruptions contribute to RIII phenotypes.[12]

However, little is known about microbiome perturbations in the small bowel after focal irradiation, largely because of the technical challenges associated with precisely targeting this area. The development of image guidance for small animal irradiators has enabled delivery of more conformal radiation dose distributions; however, the limited intrinsic soft tissue contrast of CT restricts the ability to precisely target individual bowel loops.[13] To overcome this challenge, various surgical models have been developed to irradiate bowel segments, either through surgical transposition of intestine[11] or fiducial marker placement.[14] Unfortunately, gastrointestinal surgery may impact the gut microbiome,[15] confounding efforts to define RIII-specific microbiome correlates.

Building on these methodological advances, it is crucial to evaluate whether stool samples alone can adequately capture microbiome perturbations resulting from focal RIII. Most studies seeking to understand microbiome perturbations in the context of RIII have examined stool samples.[10] However, there is growing recognition of the spatial variation of the gut microbiome along the gastrointestinal tract, known as gut biogeography.[16] Gut biogeography challenges the generalized assertion that stool microbiome profiling will fully and accurately capture microbial biomarkers of gastrointestinal disease. For example, research in inflammatory bowel disease has shown that stool microbiome profiles do not accurately represent tissue-associated microbial communities, and profiling tissue-associated microbiomes can more accurately predict disease phenotypes.[17] Gut biogeography may be particularly relevant when assessing the role of the gut microbiome in the context of small bowel RIII, because the microbiomes of the small bowel and stool are significantly different.[18]

Motivated by these challenges, we aimed to develop a noninvasive, clinically relevant focal bowel irradiation model to define the microbiome perturbations associated

with focal duodenal irradiation in both the acute and late phases of injury, and to serve as a platform for testing new RIII mitigation strategies. In addition, we aimed to uncover the relationship between duodenal and stool microbiota to evaluate the utility of stool microbiome profiling in capturing microbiome perturbations resulting from upper gastrointestinal injury.

Methods and Materials

Mice and husbandry

Mice were used in accordance with preapproved Institutional Animal Care and Use Committee protocols. Six-week-old male and female wild-type C57BL/6J mice were obtained from The Jackson Laboratory. Mice were allowed to rest 3 to 4 weeks before experimental manipulation in specific pathogen-free (SPF) housing before irradiation. After irradiation, mice were transferred to in-and-out facilities because of their inability to re-enter SPF housing. Cage changes were performed before irradiation, immediately after irradiation, at the time of stool collection, and weekly thereafter by a single laboratory member and not by animal facility personnel. For longitudinal microbiome experiments, mice were housed in groups of 4 and randomly assigned to 1 of the following 4 treatment groups to minimize cage effects: (1) 18 Gy irradiation, (2) 12 Gy irradiation, (3) iodine-sham, or (4) saline-sham. Four to 5 male and 4 to 5 female mice were used per endpoint, with the following 3 endpoints: (1) day 4, (2) day 14, and (3) day 91 after irradiation. Mice were weighed before experimental manipulation, daily for the first 4 days, and then weekly thereafter. Criteria for euthanasia included signs of hypoactivity, ataxia, shallow, rapid and/or labored breathing, pale mucous membranes, failure to groom, failure to respond to stimuli, hunched back posture, failure to drink water, losing appetite, weight loss >20% of baseline, lethargy, and not responding to social activities. A separate cohort of mice was maintained to an endpoint of 5 months after irradiation to examine histologic features of chronic RIII.

Mouse irradiation

Mice were fasted 30 minutes to 2 hours before irradiation or sham treatment. Oral gavage of 100 microliters of iodine contrast (Omnipaque 350 mg/mL, GE HealthCare) or 0.9% sterile saline was performed using plastic feeding tubes (Instech, 20 ga or 18 ga × 38 mm). After gavage, mice were placed in a Small Animal Radiation Research Platform (SARRP, Xstrahl), and anesthetized with 2% isoflurane. Cone beam computed tomography (CBCT) was performed on mice undergoing irradiation or sham treatment. A 5 × 5 mm cone was used for irradiations. Anterior to posterior/posterior to anterior (AP/PA) fields or an arc-based radiation plan consisting of 2 × 180° coplanar arcs configured to avoid the spinal cord were generated in MuriPlan software (Xstrahl) and delivered on the SARRP. Beyond initial pilot experiments, only arc-based plans were used for mouse irradiations. Mice were irradiated to either 12 Gy or 18 Gy to the proximal duodenum, just beyond the pyloric sphincter, as visualized by oral iodine contrast gavage.

Sample collection, preparation, and sequencing

Stool samples were collected into sterile Eppendorf tubes and stored at −80 °C. Stool was collected at days 4, 14, or 91 after treatment up to the endpoint for the mouse. Subsets of mice were euthanized at days 4, 14, or 91 and the proximal 1 cm of the duodenum was harvested. Dissection tools were thoroughly rinsed in ethanol, followed by cleaning with sterile isopropyl alcohol wipes between harvests from individual mice. For histologic studies, duodenal samples were generally incised lengthwise, pinned flat, and fixed overnight in 10% formalin at 4 °C. For Swiss-rolled preparation, intestinal segments from the pylorus to the ileocecal junction were harvested and prepared as previously described.[19] For longitudinal microbiome studies, duodenal samples were snap-frozen on dry ice and subsequently stored at −80 °C. Duodenal tissue was homogenized using a polytron homogenizer (Fisher Scientific) in 5.5 μL buffer/mg of tissue as previously described.[14] Buffer consisted of Pierce Ripa buffer (Thermo Scientific) containing Pierce protease inhibitor tablets (Thermo Scientific), 0.1% Tween 20 (Thermo Scientific), and 160 U/mL RNase inhibitor (Enzymatics). Homogenates were centrifuged at 14,000 rpm for 15 minutes at 4 °C and were stored at −80 °C. Genomic DNA was extracted from stool and duodenal tissue homogenates using DNeasy PowerSoil Pro Kit (Qiagen) per the manufacturer's instructions. Genomic DNA extracts from duodenal and stool samples underwent targeted amplification of the V4 region of the bacterial 16S rRNA gene, followed by multiplexed amplicon sequencing on the Illumina MiSeq platform as previously described.[20]

Bioluminescence imaging

Luminol sodium salt (Sigma-Aldrich) was dissolved in sterile phosphate-buffered saline at 60 mg/mL by vortexing. The mixture was filtered using a 0.22-μm syringe filter and covered with foil to protect from light. Mice received 300 mg/kg of luminol stock by intraperitoneal injection 5 minutes before euthanasia. Mice were anesthetized with 2% isoflurane and euthanized by cervical dislocation, and intestinal samples were harvested as above. Samples were imaged immediately after harvest with an In Vivo Imaging System SpectrumCT (PerkinElmer), using an open filter setting and a 5-minute exposure.

BrdU assay

A subset of mice were irradiated to a dose of 12 or 18 Gy as above, and in vivo BrdU assay was performed 72 hours after irradiation. Ninety minutes before euthanasia, mice received an intraperitoneal injection of 10 μL/g BrdU labeling reagent (Invitrogen). Proximal duodenal tissue samples were harvested as above for histology.

Histology

Embedding, sectioning, and staining were performed by the Digestive Disease Research Core Center at Washington University in Saint Louis. Longitudinal, formalin-fixed tissue samples were trimmed and stabilized in 2% agar for subsequent paraffin embedding and sectioning. Masson's trichrome stain was performed according to standard protocols. BrdU immunohistochemistry (IHC) (rat monoclonal antibody, Accurate Chemical & Scientific Corporation) and γH2AX IHC (rabbit monoclonal, Bethyl Laboratories) were performed according to standard protocols with hematoxylin counterstain. Slides were scanned for analysis using a VS120 Olympus Slide Scanner at 20 × magnification.

Data analysis and statistics

BrdU and weight data were analyzed in Prism10 using a one-way analysis of variance with Tukey's multiple comparisons correction. IHC staining for γH2AX was quantified using QuPath[21] and analyzed in Prism10 using Student *t* tests. Illumina amplicon 16S rRNA sequencing data were processed as previously described,[20] using the DADA2 package in R.[22] Bacterial taxonomy was assigned using the Silva version 138.1 reference database.[23] Data were filtered to retain taxa with a minimum relative abundance of 0.1%. The Vegan R package was used to calculate sample richness.[24] Mean diversity scores were compared using pairwise Wilcoxon tests with Benjamini-Hochberg correction. The phyloseq,[25] phanghorn,[26] and Vegan R packages were used to calculate and ordinate weighted UniFrac distances between samples. The adonis2[27] and pairwise.adonis2[28] R packages were used to calculate PERMANOVAs (Permutational Multivariate Analysis of Variance). MaAsLin2 linear mixed modeling R package was used to identify significantly enriched or depleted bacterial taxa among treatment groups.[29]

Results

Oral iodine contrast enables visualization of the duodenum to facilitate focal irradiation

Onboard CBCT on a small animal irradiator provided limited soft tissue contrast to identify individual bowel loops, as shown in Figure 1A left. Administration of iodine contrast by oral gavage just before CBCT allowed for visualization of the stomach and proximal duodenum (Fig. 1A right). Because of continuous transit of contrast through the gastrointestinal tract, we investigated how intraduodenal contrast (present vs absent) impacted the required treatment time to achieve the prescription radiation dose. For an 18 Gy treatment, the percentage increase in total beam time with contrast was 2% ± 1.7% (N = 3). This indicates that the presence or absence of contrast in the intestine likely has little effect on the tissue dose.

With improved visualization of the proximal duodenum, we developed 2 treatment plans to irradiate the proximal 5 mm of the duodenum (Fig. 1B). The top panel shows isodose lines for a 5 × 5 mm AP/PA beam arrangement. In this arrangement, the 100% isodose line spans the entire sagittal plane along the path of the beams. To reduce high-dose spill into surrounding tissues, we developed a conformal arc plan consisting of 2 coplanar 180° arcs configured to avoid dose to the spinal cord, as shown in Figure 1B bottom.

To macroscopically assess our ability to successfully irradiate the proximal duodenum, we employed luminol bioluminescence imaging at the time of euthanasia, 4 days after irradiation. Luminol has been shown to luminesce in proportion to myeloperoxidase activity,[30] which is increased after radiation tissue injury,[31,32] and following focal RIII.[33] Increased luminol bioluminescence was observed in the proximal duodenum, indicating successful irradiation of our target volume (Fig. 1C). Interestingly, we observed bioluminescence outside of the proximal duodenum in the mouse irradiated with the AP/PA arrangement.

To further compare spatial dose localization between the 2 beam arrangements, we assessed DNA double-strand breaks within intestinal segments from the pylorus to the ileocecal junction using γH2AX IHC. We irradiated the proximal duodenum of C57BL/6J mice using either an AP/PA or arc plan (N = 4/group) and collected tissues 2 hours later in a Swiss-rolled fashion (Fig. 1D/E). Although γH2AX IHC does not allow for absolute dose quantification across tissue sections, it reliably delineates irradiated regions in complex specimens.[34] Quantification of staining using QuPath showed no significant differences between the 2 plans in either percent positive cell nuclei (≥1+) or histochemical score (H-score)[35] (Fig. 1F). We used the conformal arc plan for subsequent experiments because it more closely replicates SABR therapy delivery.

Focal irradiation to the proximal duodenum produces focal radiation injury and is well tolerated

We next measured the number of proliferative intestinal cells and crypts, which are depleted by radiation injury, using a BrdU assay. Wild-type C57BL/6J mice (N = 3/group) received 12 or 18 Gy to the proximal 5 mm of the

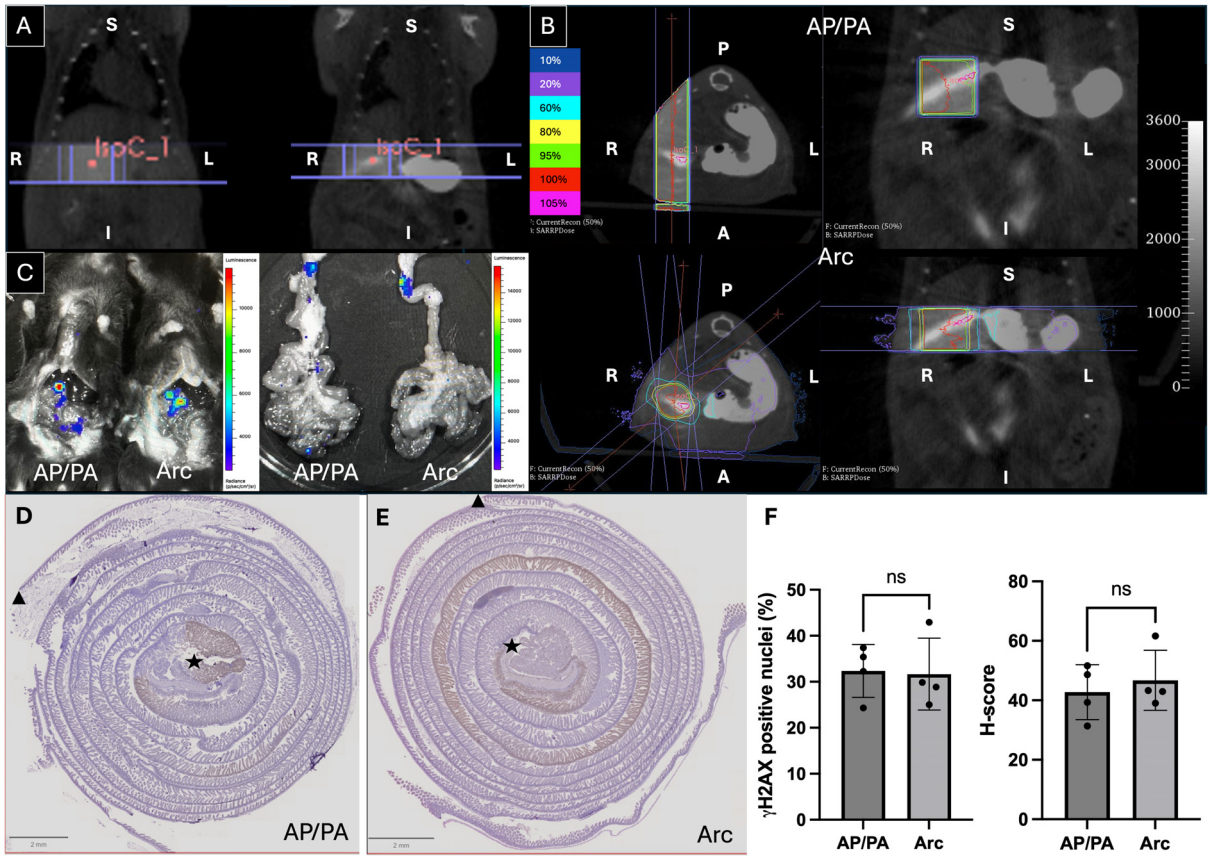

Fig. 1. Oral iodine contrast enables visualization of the proximal duodenum to facilitate focal duodenal radiation. (A) CT without (left) and with (right) oral iodine contrast (Omnipaque 350 mg/mL, GE HealthCare) given just before imaging. (B) Small animal irradiator treatment plan using AP/PA beam arrangement (top) and an arc plan (bottom) to enable focal irradiation to the proximal duodenum. (C) Luminol (300 mg/kg, IP 5 minutes before euthanasia) enabled visualization of myeloperoxidase activity in irradiated tissues. γH2AX immunohistochemistry micrographs of Swiss-rolled small intestinal segments after irradiation of the proximal duodenum to 18 Gy using AP/PA (D) or Arc (E) plans. (F) Quantification of percent positive cell nuclei (≥1+) and histochemical score (H-score) in each treatment group. Image orientation: A-anterior, P-posterior, S-superior, I-inferior, R-right, L-left, proximal small intestine (star), and distal small intestine (triangle). *Abbreviations:* AP/PA = anterior to posterior/posterior to anterior; CT = computed tomography; IP = intraperitoneal; SARRP = Small Animal Radiation Research Platform; H2AX = H2A histone family member X; ns = nonsignificant.

duodenum, and an in vivo BrdU assay was performed 3 days after irradiation. Focal intestinal irradiation at 12 and 18 Gy has been shown to be well tolerated based on previous work.[14] Figure 2A-C shows representative immunohistochemical sections of the untreated, 12 Gy, and 18 Gy-irradiated duodenum, respectively. Unirradiated duodenum shows robust BrdU crypt staining representing proliferating crypt cells, whereas irradiated portions of the duodenum show reduced BrdU crypt staining. To quantify BrdU differences, the total number of BrdU-positive cells/crypt and the percentage of regenerating crypts, defined as crypts containing 5 or more BrdU +cells,[6] were compared across treatment groups by evaluating 50 crypts in the proximal 5 mm of the duodenum of each mouse. There was a significant decrease in both the number of BrdU-positive cells per crypt (12 Gy $P < .05$, 18 Gy $P < .01$) and the number of regenerating crypts in the irradiated duodenum compared to the unirradiated duodenum (12 Gy/18 Gy, $P < .001$) (Fig. 2D). There were no significant differences between the 12 and 18 Gy groups. This contrast in BrdU staining between the irradiated and unirradiated portions of the duodenum was starkly apparent in a representative mouse section irradiated to 18 Gy, as shown in Figure 2E. Overall, this demonstrates our ability to model focal radiation injury in the proximal duodenum.

We next sought to ascertain the tolerance of focal duodenal irradiation. Wild-type C57BL/6J mice (5 male and 5 female mice, N = 10/treatment) received 12 or 18 Gy to the proximal 5 mm of the duodenum. At 91 days after irradiation, all mice survived, and during this period, they continued to gain weight with no differences compared with sham-treated controls (Fig. 2F, $P > .05$). In a separate experiment, mice were euthanized at 5 months postirradiation to determine the ability of our model to elicit late effects of focal radiation injury. Trichome staining of a section of the proximal duodenum shows villous atrophy, crypt

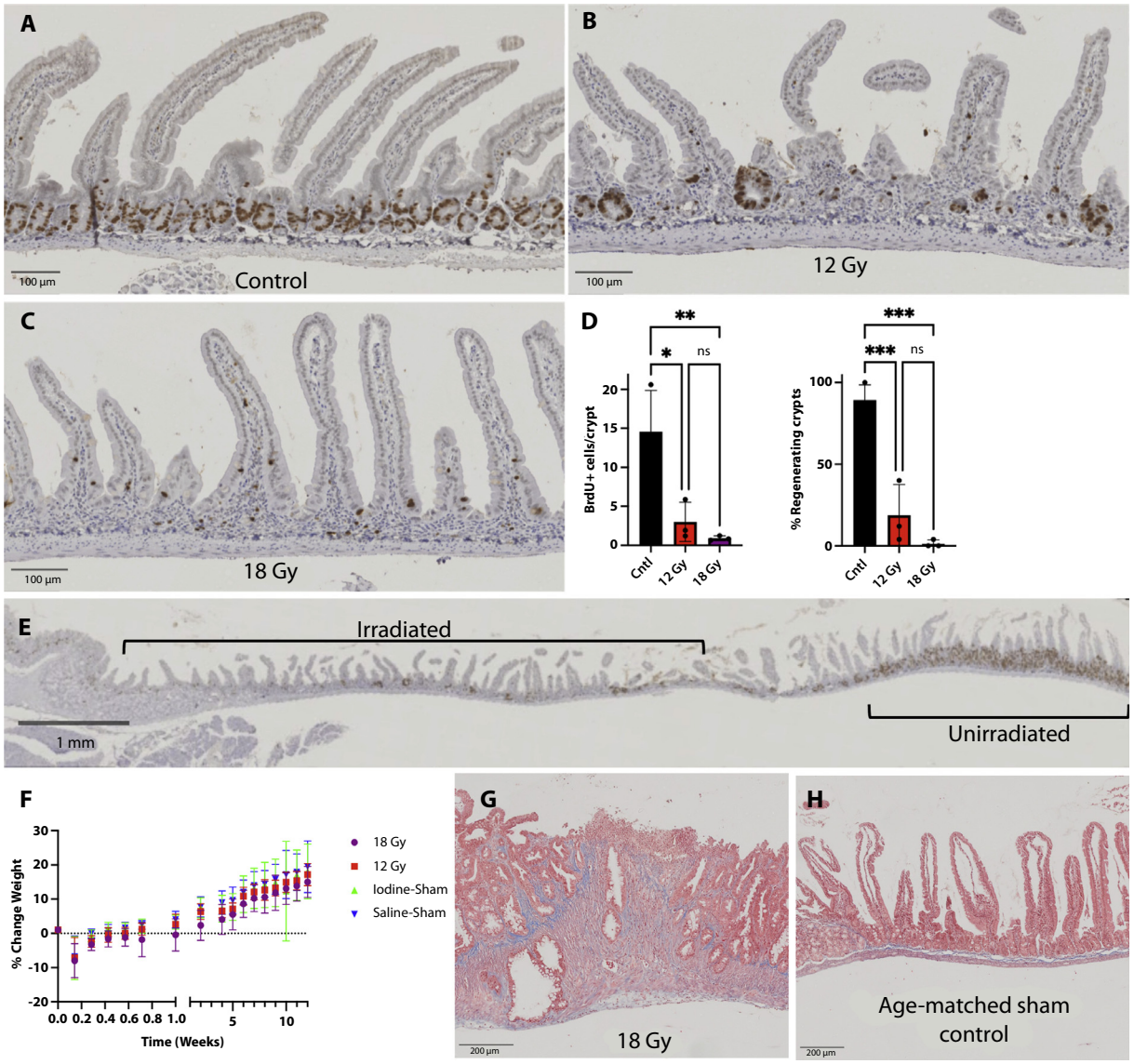

Fig. 2. Focal duodenal irradiation is well tolerated and induces localized acute and late radiation injury. (A−C) Representative immunohistochemical micrographs of the proximal duodenum from wild-type C57BL/6J mice, demonstrating BrdU crypt staining in (A) unirradiated controls and specimens irradiated with (B) 12 Gy and (C) 18 Gy at 3 days after irradiation. (D) Quantification of BrdU-positive cells per crypt and the percentage of regenerating crypts (defined as crypts with ≥5 BrdU-positive cells) across 50 crypts in the irradiated duodenum compared to the unirradiated region (One-way ANOVA with Tukey's multiple comparisons test, $^{*}P < .05$, $^{**}P < .01$, $^{***}P < .001$). (E) A representative 18 Gy-irradiated duodenal section contrasting BrdU staining in the irradiated area (left) against the adjacent unirradiated tissue (right). (F) Tolerance to treatment is assessed by weight change. (G−H) At 5 months postirradiation, trichrome staining of the proximal duodenum reveals late-phase radiation injury characterized by villous atrophy, crypt hyperplasia, and submucosal fibrosis in irradiated mice (G), as compared with age-matched sham-treated controls (H). *Abbreviation:* BrdU = Bromodeoxyuridine; Cntl = control; ns = nonsignificant; ANOVA = analysis of variance.

hyperplasia, and submucosal fibrosis characteristic of late radiation injury (Fig. 2G) compared with age-matched sham-treated control (Fig. 2H). Altogether we demonstrate that our focal duodenal irradiation model produces acute and late-phase radiation injuries that are well tolerated, owing to the clinically relevant dose distribution and noninvasive technique.

Focal irradiation to the proximal duodenum leads to changes in bacterial beta diversity in the duodenum but not the stool

Having demonstrated that our model produces localized duodenal injury, we sought to understand how focal duodenal irradiation perturbs the duodenal and stool microbiomes,

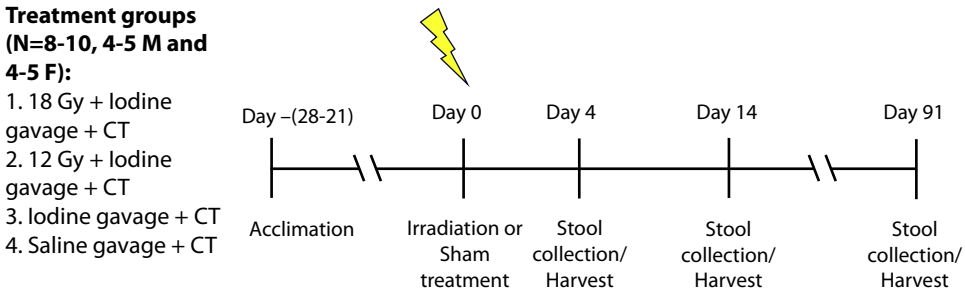

Fig. 3. Experiment schema. *Abbreviation:* CT = computed tomography; M = male; F = female.

with the hypothesis that focal radiation injury would elicit local and biogeographically distinct microbiome perturbations. Wild-type C57BL/6J mice (N = 8-10 M/F /treatment/ time point, total = 112) received 12 or 18 Gy to the proximal 5 mm of the duodenum (Fig. 3). To account for potential confounding variables, control groups underwent sham treatment with either iodine contrast gavage followed by CT (Iodine-Sham) or saline gavage followed by CT (Saline-Sham). Duodenal and stool samples were collected at days 4, 14, and 91 postirradiation for 16S rRNA gene sequencing. To ensure adequate sequencing depth for microbial diversity analysis, we performed rarefaction to identify the per-sample sequencing depth required to include samples in diversity comparisons. We determined that approximately 5000 reads were sufficient for duodenal samples (Fig. E1A), whereas 15,000 reads were adequate for stool samples (Fig. E1B).

We next sought to examine the alpha and beta diversity of the bacterial communities in the duodenum and stool. Globally, there were differences in the alpha and beta diversity between the pooled (all time points) duodenal and stool samples as quantified by richness, evaluated at the taxonomic level of genus, and weighted UniFrac distances, respectively. Stool samples had increased richness compared to duodenal samples, as shown in Figure 4A (Wilcoxon, $P < .0001$), consistent with previous reports.[36] In addition, principal coordinate analysis (PCoA) of between sample weighted UniFrac distances showed that the microbial compositions of the duodenum and stool were distinct (PERMANOVA, $P = .001$) (Fig. 4B).

We also compared the alpha and beta diversity of bacterial communities between our treatment groups in both the duodenum and stool. There was no difference in bacterial richness between the saline-sham control group and any other treatment group in the duodenal samples (Wilcoxon, $P > .05$) (Fig. 4C, E; Fig. E2). The PCoA clustering of weighted UniFrac distances indicates treatment group-specific sample distribution, and PERMANOVA analyses of weighted UniFrac distances were statistically significant by the treatment group (PERMANOVA, $P < .05$) (Fig. 4D).

To evaluate when irradiation-induced microbiome perturbations within the duodenum were most pronounced, weighted UniFrac distances were compared between treatment groups at each time point (Fig. 4F and Fig. E3). Subsetting the data by endpoint suggested that the aggregate differences in beta diversity between treatment groups were largely driven by the day 4 samples. PERMANOVA analysis of weighted UniFrac distances between treatment groups at day 4 is significant ($P < .01$) (Fig. 4F). Visual inspection of the PCoA plots in Figure 4F shows 2 distinct clusters, with 1 cluster that includes the sham-treated groups and the other cluster including the irradiated groups. This was consistent with pairwise PERMANOVA, which showed statistically significant differences in the saline-sham versus 12 or 18 Gy treated mice (PERMANOVA, adjusted $P < .01$) and between the iodine-sham group versus 12 or 18 Gy (PERMANOVA, adjusted $P < .05$). There were no differences between the 12 Gy versus 18 Gy groups (PERMANOVA, adjusted $P > .05$). PERMANOVA of the weighted UniFrac distances of duodenal samples at days 14 and 91 (Fig. E3) showed no significant differences between treatment groups ($P > .05$). There were no significant differences in stool richness or weighted UniFrac distances between treatment groups at day 4 after irradiation as shown in Figure 4G and H, respectively, or any other endpoint (Fig. E2 and E3). Altogether, these results demonstrate dose- and time-dependent radiation-induced perturbations in bacterial community diversity that are apparent in the duodenal microbiome without corresponding differences in the stool microbiome.

Focal duodenal irradiation induces dose- and time-dependent microbiome perturbations in the duodenum that are not detectable in the stool

There were apparent qualitative differences between the relative abundance of bacterial genera in duodenum (Fig. 5A) and stool (Fig. 5B). To ascertain differences in bacterial taxa between treatment groups at each time point, we employed multivariable association modeling with MaAsLin2. After accounting for potential confounding variables including sex, cage, and sequencing run, we identified dose- and time-dependent microbiome perturbations relative to saline-sham controls at days 4 and 14 posttreatment in the duodenum as shown in Figure 6A. In the mice irradiated to 18 Gy, there was significant size effect differences at multiple taxonomic classifications including 5 genera, 8 families, and 5 phyla (Fig. 6A). Notably, there was an 18 Gy treatment group-specific increase in the Akkermansiaceae family at

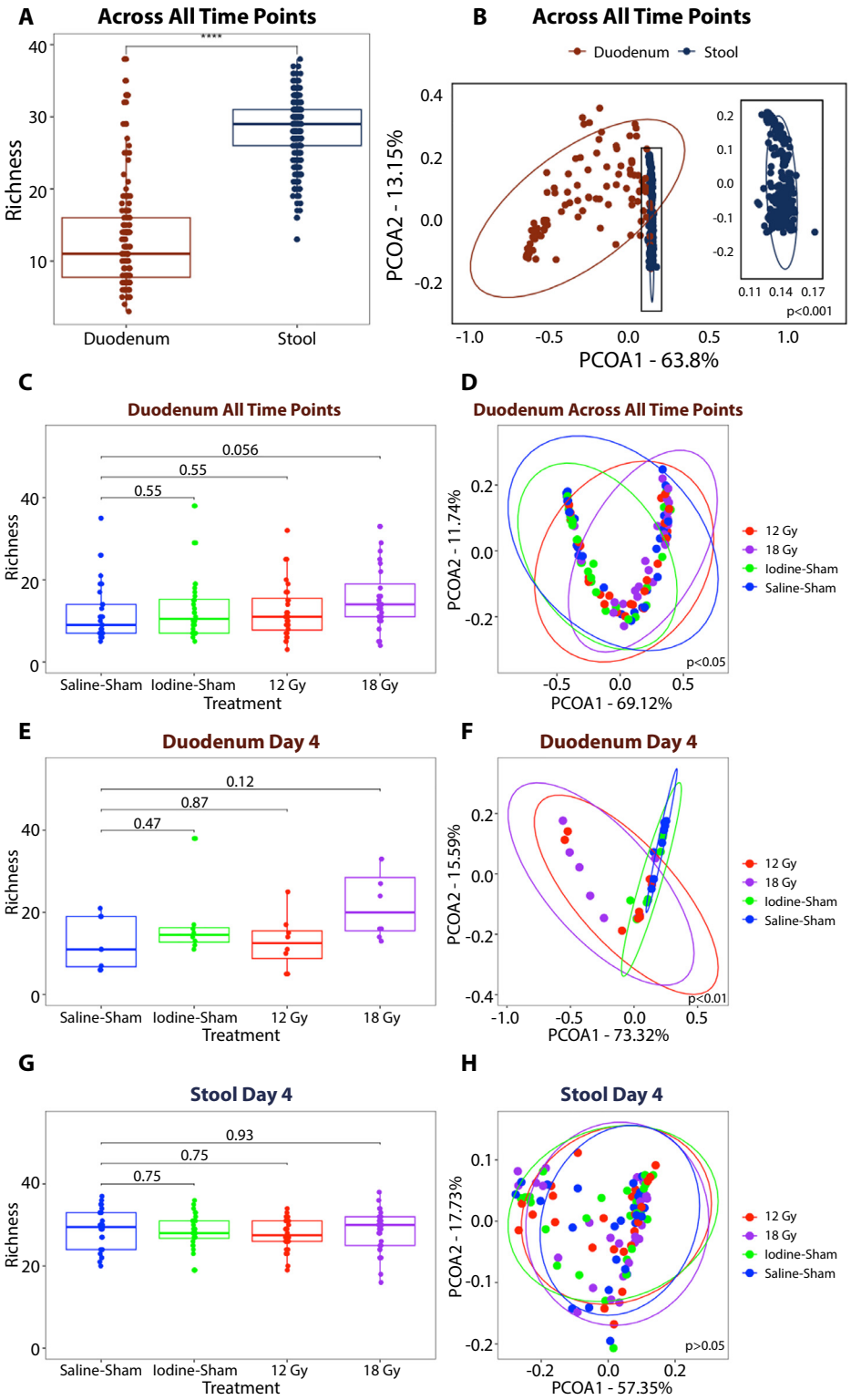

Fig. 4. Radiation-induced alterations in gut microbiome diversity. (A) Alpha diversity as measured by bacterial richness of pooled duodenal and stool samples across time points (Wilcoxon, $^{****}P < .0001$). (B) Principal coordinate analysis (PCoA) of weighted UniFrac distances between duodenal and stool samples (PERMANOVA, $P < .001$). (C) Duodenal bacterial richness across treatment groups from pooled time points compared to saline-sham controls (Wilcoxon, BH-corrected). (D) PCoA of weighted UniFrac distances among treatment groups from pooled time points (PERMANOVA, $P < .05$). (E) Analysis of bacterial richness (Wilcoxon, BH-corrected) and (F) PCoA of weighted UniFrac distances among treatment groups in the duodenum at day 4 posttreatment (PERMANOVA, $P < .01$). (G) Bacterial richness (Wilcoxon, BH-corrected) and (H) PCoA of weighted UniFrac distances among treatment groups in the stool at day 4 (PERMANOVA, $P > .05$). *Abbreviation:* PERMANOVA = Permutational Multivariate Analysis of Variance; BH = Benjamini-Hochberg.

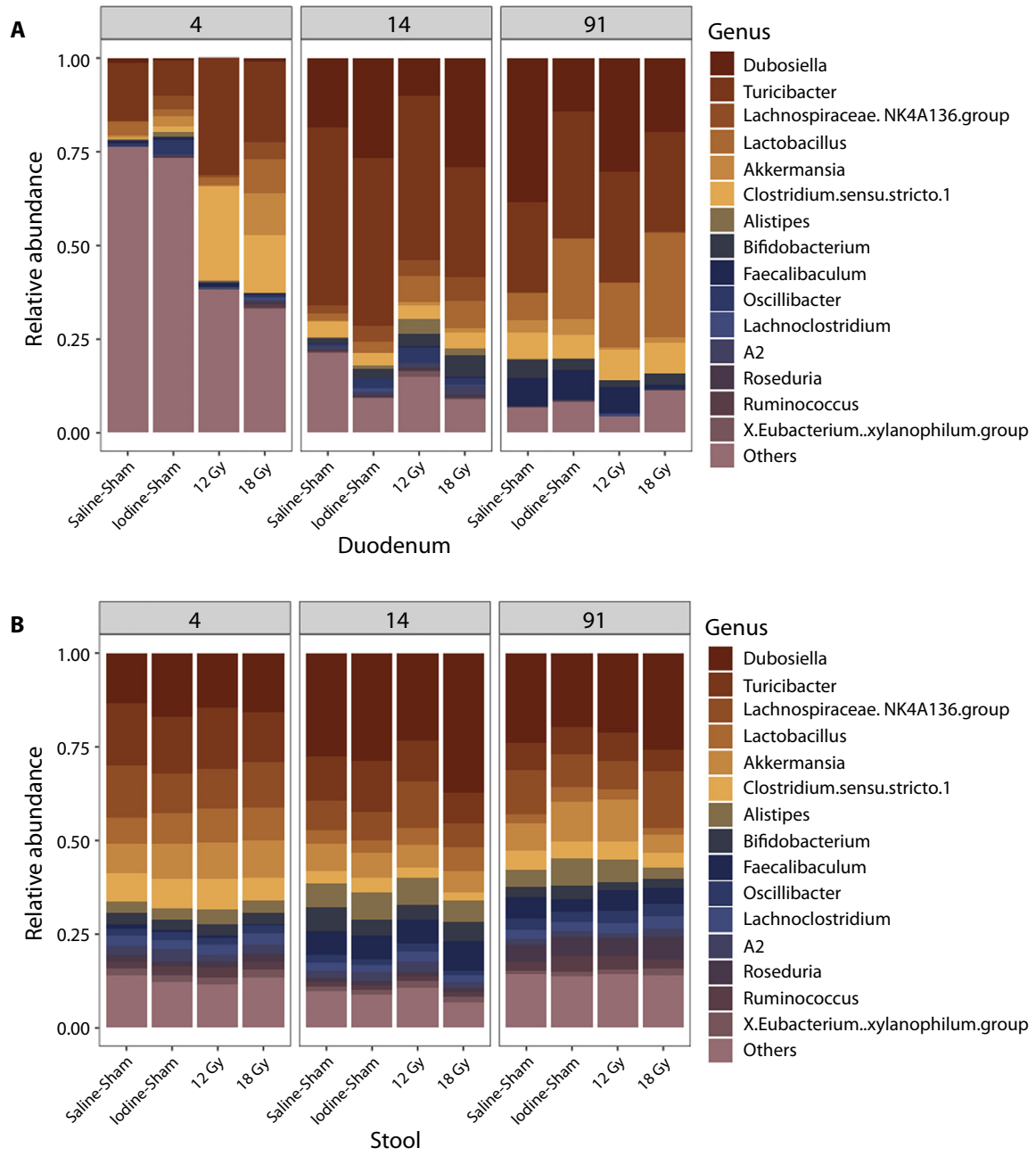

Fig. 5. Relative abundance of bacterial genera by time and treatment groups in the (A) duodenum and (B) stool.

days 4 ($P < .01$) and 14 ($P < .01$) posttreatment and the Lactobacillaceae family at day 4 posttreatment ($P < .05$).

In both the 12 Gy and 18 Gy duodenal samples, there were concordant increases in the relative abundance of Clostridium.sensu.stricto.1 genera, Clostridiacea family, and Firmicutes phylum, and a consistent decrease in the relative abundance of Proteobacteria phylum at day 4 after irradiation and a decrease in the relative abundance of Xanthobacteraceae family at day 14 after irradiation. There was only 1 change that was consistent among all groups of mice that received iodine contrast (iodine-sham, 12 Gy, 18 Gy), and that was an decrease in Actinobacteriota at day 4, suggesting that receiving oral iodine contrast does not cause substantial perturbation of the duodenal microbiome. Lastly, there were only 2 significant taxonomic size effect differences observed in the stool of irradiated mice, an increase in *Lactobacillus* at both the genus and family level at day 14 in the 18 Gy group ($P < .001$) (Fig. 6B). Overall, these results demonstrate dose- and time-dependent duodenal microbiome perturbations after focal duodenal irradiation that are almost completely absent from the stool microbiome.

Discussion

The toxicity of radiation is a function of the dose and volume of irradiated tissue.[37] In the setting of widespread adoption of intensity modulated radiation therapy, there is

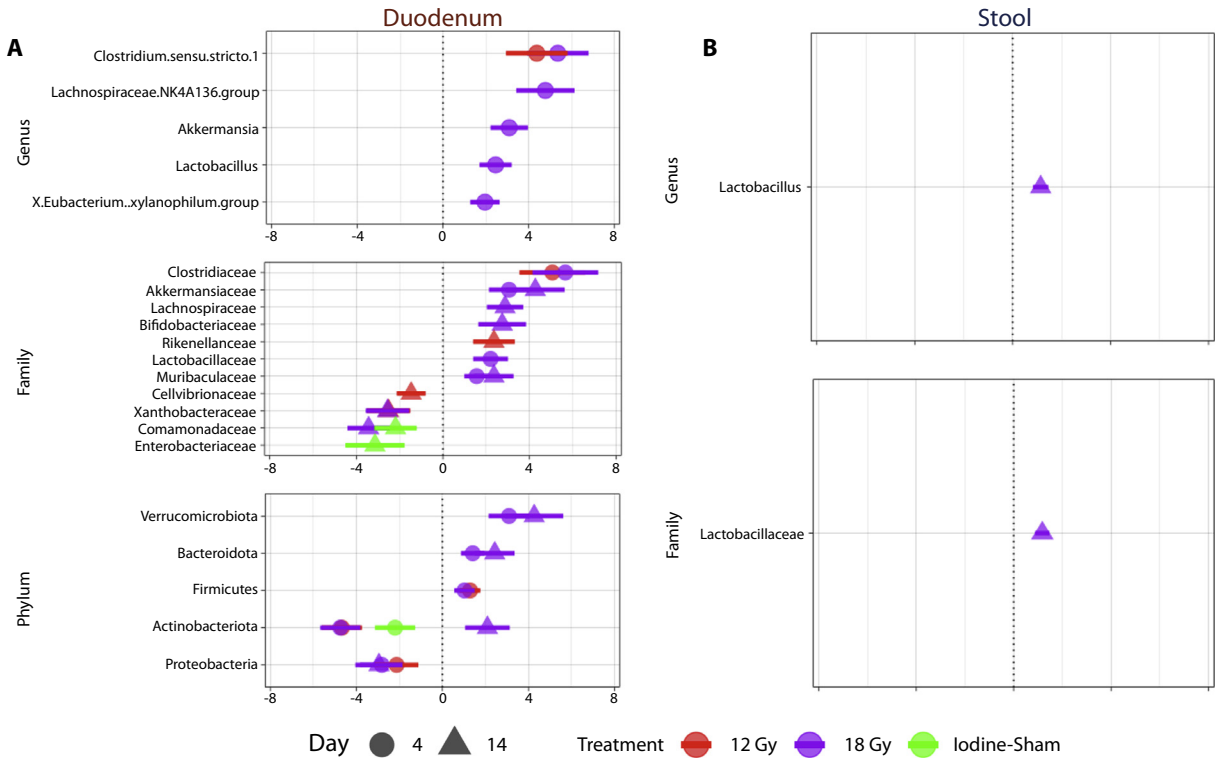

Fig. 6. Dose- and time-dependent duodenal microbiome perturbations revealed by multivariable association modeling using MaAsLin2. (A) After controlling for potential confounders (sex, cage, and sequencing run), we identified bacterial taxa that were differentially abundant after focal duodenal irradiation in the (A) duodenum and (B) stool microbiomes relative to saline-sham control at days 4 and 14 after treatment. There were no differentially abundant taxa at 91 days after irradiation.
Abbreviation: MaAsLin2 = Microbiome Multivariable Associations with Linear Models 2.

increasing utilization of hypofractionation and SABR.[38] Recapitulating the dose distributions used in these treatment paradigms, characterized by higher dose per fraction and more conformal volumes,[39] will be critical to establishing relevant preclinical models to optimize the therapeutic ratio of hypofractionation and SABR in the clinic. A key challenge in preclinical models of RIII is delivering high-radiation doses without compromising survival, thereby allowing sufficient time for the development of late effects. This limitation may hinder our understanding of the mechanisms driving late toxicity in patients undergoing abdominopelvic radiation therapy.[11]

Most preclinical studies investigating RIII rely on TBI or WAI.[10] The lethal dose for 50% of mice at 10 days following WAI is approximately 15.6 Gy.[40] Here, we report a simple and noninvasive method of focal bowel irradiation that is well tolerated, with 100% of mice surviving irradiation to 18 Gy at 91 days after treatment. Single-fraction pancreas SBRT represents a clinically analogous scenario for our model. In the Stanford single-fraction SBRT series, a dose constraint of 5% of the volume receiving <22.5 Gy was applied,[41] significantly exceeding the tolerable doses achievable with WAI. This comparison is particularly relevant given that the duodenum in mice is approximately 7 cm long,[42] meaning our 5 × 5 mm irradiation field targets about 7% of the total duodenal volume. Supporting this approach, previous studies suggest that higher doses of single-fraction focal irradiation to the small intestine may be tolerated and would more accurately reflect clinically relevant doses.[14]

Focal irradiation of the small bowel has been achieved in murine and rat models using either surgical exteriorization of the intestine[43] or transposition of the small bowel into the scrotum.[11] More recently, Verginadis et al[14] demonstrated that surgical implantation of a fiducial marker enabled focal irradiation to the jejunum using a small animal irradiator with CBCT guidance. This procedure was well tolerated, with 86% of mice surviving up to 120 days after treatment. This model was able to recapitulate histologic features of chronic RIII, notably fibrosis, immune cell infiltration, and dysmorphic tissue architecture.[14] A potential pitfall of these approaches in the context of characterizing radiation-specific perturbations of the microbiome is that gastrointestinal surgery can itself lead to microbiome perturbations.[44]

Our method does not require surgical manipulation. Using oral iodine contrast enabled visualization of the stomach and duodenum, allowing for delivery of conformal high-dose radiation to the proximal duodenum. Oral iodine contrast itself may be used clinically at the time of radiation simulation for delineation of the small bowel, and so this additional experimental manipulation is

clinically reasonable.[45] Standardization of oral iodine contrast kinetics may allow for irradiation of other segments of the intestine. Alternatively, we found that iodine contrast enema after clearing of colonic stool pellets enabled rapid visualization of the colon and the terminal ileum (Fig. E4). Altogether our method should allow for facile delivery of high-dose focal radiation to intestinal segments, which we hope will accelerate mechanistic and interventional preclinical and translational studies seeking to mitigate RIII.

We used our novel murine model to investigate the impact of focal duodenal irradiation on the microbiome in both the duodenum and stool, an inquiry that existing preclinical models have been unable to address. Despite the duodenum being a critical organ at risk during abdominal radiation therapy,[46] its microbiome perturbations in this setting remain largely undefined. Numerous preclinical and clinical studies have sought to characterize microbiome perturbations associated with RIII by examining community-level bacterial diversity and assessing differentially abundant bacterial taxa after radiation injury, primarily sampling stool after TBI or WAI.[10] Reports of differentially abundant bacterial taxa associated with abdominopelvic radiation have varied across preclinical studies. However, a systematic review by Fernandes et al[10] identified that Proteobacteria, Verrucomicrobia, *Alistipes, and Akkermancia* were most consistently observed to be relatively more abundant in the gut following irradiation, whereas Bacteroidetes, Firmicutes, and *Lactobacillus* were typically found to be reduced.

Our findings highlight a significant knowledge gap, demonstrating time- and dose-dependent microbiome changes under clinically relevant conditions that preclinical WAI models cannot replicate because of high rates of attrition. We identified specific bacterial taxa that were differentially abundant in the duodenal tissue of mice subjected to focal duodenal irradiation. Most of these taxa were observed in mice that received 18 Gy (Fig. 6A). Notably, at days 4 and 14 after irradiation, there was a higher relative abundance of commensal taxa, including *Akkermansia, Lactobacillus, Lachnospiraceae NK4A136 group, Eubacterium xylanophilum group*, Bifidobacteriaceae, and Muribaculaceae (Fig. 6A). The increase in *Akkermansia* aligns with previous reports, whereas the increase in *Lactobacillus* contrasts with earlier studies.[10] Consistent with our hypothesis that microbiome perturbations after focal irradiation are spatially confined, we detected only 2 taxa at a significantly altered relative abundance in the stool after focal irradiation, an increase in *Lactobacillus* genus/family at 14 days posttreatment. This could represent limited propagation of microbial perturbations from the initial site of injury.

Most of the differentially abundant taxa represent anaerobes or facultative anaerobes and are also found in the stool (Table E1-E3). This runs contrary to the hypothesis that bacterial taxa associated with duodenal radiation injury are biogeographically distinct. Work by Alam et al[47] helps to contextualize these findings. In their work, they developed an endoscopic colonic mucosal wound model to define microenvironmental influences of wound healing in the gut. They observed that rapid local depletion of oxygen in the mucosal wound promoted robust growth of anaerobic bacteria, notably *Akkermansia* and *Lactobacillus*, and was dependent on formyl peptide receptor 1 and neutrophilic NADPH oxidase. They additionally demonstrated that *Akkermansia* promoted wound healing in an formyl peptide receptor 1−dependent manner. In our work, we observed an increase in the relative abundance of *Akkermansia* at days 4 and 14 postirradiation in the *duodenum*; however, we do not see a concordant change in the *stool*. Given the aforementioned study suggesting a beneficial role for *Akkermansia* in mucosal healing, wound-associated *Akkermansia* may represent an important prognostic microbial biomarker of RIII, and supplementation may facilitate tissue repair as has been suggested.[48]

Interestingly, microbiome perturbations in our model diminish over time, with no significant changes at 91 days posttreatment. Unfortunately, the design of our study does not facilitate dynamic monitoring of the duodenal microbiome; however, noninvasive sampling of gut microbiota has been described[49] and may be considered for future preclinical and translational studies. This may be particularly important in understanding microbiome perturbations in the small bowel, given that the small intestine microbiome composition is more dynamic compared to the large intestine.[50] Large interindividual variations in the small intestine microbiome have been reported over a period of 9 to 28 days,[51] which may account for temporal variation in the relative abundance of bacterial genera in the saline-sham and iodine-sham controls.

Our experimental design may also account for the absence of microbiome differences in irradiated and control mice at 91 days after treatment. Although we attempted to control for confounding experimental variables such as environmental exposures, sex, and cage effects, the impact of cohousing mice from different treatment groups in the same cage may dilute treatment-related microbiome phenotypes because of coprophagy.[52] An alternative approach for future studies would be to use multiple cages of similarly treated mice in small numbers (2 per cage), which may increase the power to detect microbiome perturbations after treatment.[52]

Another novel finding of this study was describing the impact of oral iodine contrast on the gut microbiome, which to our knowledge has never been defined in vivo. It has been hypothesized that oral iodine contrast may perturb the gut microbiome because of iodine's antiseptic properties[53]; however, we only see 3 differentially abundant taxa in the iodine-sham group compared with saline-sham control and only 1 concordant changes among all the groups that received iodine (iodine-sham, 12, 18 Gy), suggesting that oral iodine contrast administration has little influence on the microbiome perturbations observed in our model.

The generalizability of our findings is limited by the challenges of maintaining mice under SPF conditions after irradiation and the use of a single mouse strain from a single vendor. Because SPF housing was not feasible after SARRP

irradiation, we implemented robust sham controls with identical exposures to account for environmental variables. Environmental factors and husbandry are known to strongly influence microbiome phenotypes.[54] Nevertheless, we consistently observed duodenal-specific microbiome perturbations across multiple timepoints that were not reflected in stool. We acknowledge that the specific taxa affected may vary with husbandry conditions and by mouse strain and vendor.

Another limitation is the exclusion of tumors from our model, which allowed us to examine late RIII endpoints without the confounding risk of tumor-related mortality. However, this distinction is important as significant microbiome perturbations have been documented in patients with gastrointestinal tumors both in the duodenum[55] and stool.[56] The development of defined gastrointestinal communities that approximate the baseline microbiome of patients with cancer may help standardize preclinical studies across laboratories. Moreover, it remains important to assess how modulation of the microbiome to mitigate RIII influences tumor kinetics.

Additional avenues for future study include correlating microbiome phenotypes with markers of radiation injury including histology, metabolomics, and profiling of the immune and inflammatory landscapes in acute and late radiation injury. This may help to further define host-microbiome interactions that drive RIII. Moreover, we report herein the changes in the relative abundance of bacteria based on 16S rRNA gene sequencing; however, recent work has demonstrated that absolute bacterial loads may be an important confounding variable that impacts microbiome-disease correlates.[57] In addition, it has been suggested that distinguishing the "viable" fraction of microbiota in a sample may be important for elucidating microbiome phenotypes.[58] Future work should consider not only the relative abundance of bacterial taxa observed after RIII but also absolute abundances and the viable fraction of samples. Furthermore, age is an important modifying factor of both RIII and the gut microbiome,[59] with older mice demonstrating higher sensitivity to RIII.[60] Because we used adolescent mice in our study, future work should systematically evaluate the interaction of age, RIII, and the gut microbiome. Lastly, the fungal and bacterial microbiomes differentially regulate radiation treatment efficacy[61]; however, little is known about the influence of the fungal microbiome on RIII. Prophylactic fluconazole administration abrogates the toxicity of radiation mucositis in patients with head and neck cancer undergoing radiation treatment,[62] suggesting a potential protective role of antifungal treatment. Further studies should seek to understand the role of the fungal microbiome in the context of RIII.

Conclusions

Our clinically relevant focal duodenal radiation injury model is safe, well tolerated, and easy to implement. It enables characterization of microbiome perturbations during both the acute and late phases of injury and can serve as a platform for testing new RIII mitigation strategies. We identified dose-, time-, and spatially dependent microbiome perturbations after RIII in the duodenal tissue that were not apparent in stool. Our data underscore the imperative of directly assessing tissue-associated microbiota, as relying solely on stool samples risks overlooking critical, localized microbial dynamics that may drive injury and repair. Bridging the gap in our understanding of the impacts of the microbiome on RIII may uncover new insights to enhance the therapeutic ratio of radiation therapy.

Declaration of generative AI in scientific writing

During the preparation of this work, LHG used [ChatGPT4o/ OpenAI] in order to (1) generate code in R for analysis and plotting of microbiome data, and (2) assist in editing selected portions of the manuscript to improve clarity and conciseness. After using this tool/service, LHG reviewed and edited the content as needed. All authors have reviewed the final manuscript and take full responsibility for the content of the publication.

References

1. Delbaere K, Roegiers I, Bron A, et al. The small intestine: Dining table of host-microbiota meetings. *FEMS Microbiol Rev* 2023;47:fuad022.
2. Zindler JD, Thomas Jr CR, Hahn SM, et al. Increasing the therapeutic ratio of stereotactic ablative radiotherapy by individualized isotoxic dose prescription. *J Natl Cancer Inst* 2016;108:djv305.
3. Moraitis I, Guiu J, Rubert J. Gut microbiota controlling radiation-induced enteritis and intestinal regeneration. *Trends Endocrinol Metab* 2023;34:489-501.
4. Crawford PA, Gordon JI. Microbial regulation of intestinal radiosensitivity. *Proc Natl Acad Sci U S A* 2005;102:13254-13259.
5. Zhao Z, Cheng W, Qu W, Shao G, Liu S. Antibiotic alleviates radiation-induced intestinal injury by remodeling microbiota, reducing inflammation, and inhibiting fibrosis. *ACS Omega* 2020;5:2967-2977.
6. Ciorba MA, Riehl TE, Rao MS, et al. Lactobacillus probiotic protects intestinal epithelium from radiation injury in a TLR-2/cyclo-oxygenase-2-dependent manner. *Gut* 2012;61:829-838.
7. Xie LW, Lu HY, Tang LF, et al. Probiotic consortia protect the intestine against radiation injury by improving intestinal epithelial homeostasis. *Int J Radiat Oncol Biol Phys* 2024;120:189-204.
8. Guo H, Chou WC, Lai Y, et al. Multi-omics analyses of radiation survivors identify radioprotective microbes and metabolites. *Science* 2020;370:eaay9097.
9. Liu MM, Li ST, Shu Y, Zhan HQ. Probiotics for prevention of radiation-induced diarrhea: A meta-analysis of randomized controlled trials. *PloS One* 2017;12:e0178870.
10. Fernandes A, Oliveira A, Soares R, Barata P. The effects of ionizing radiation on gut microbiota: What can animal models tell us?-A systematic review. *Curr Issues Mol Biol* 2023;45:3877-3910.
11. Hauer-Jensen M, Poulakos L, Osborne JW. Effects of accelerated fractionation on radiation injury of the small intestine: A new rat model. *Int J Radiat Oncol Biol Phys* 1988;14:1205-1212.
12. Gerassy-Vainberg S, Blatt A, Danin-Poleg Y, et al. Radiation induces proinflammatory dysbiosis: Transmission of inflammatory susceptibility by host cytokine induction. *Gut* 2018;67:97-107.

13. Verhaegen F, Granton P, Tryggestad E. Small animal radiotherapy research platforms. *Phys Med Biol* 2011;56:R55-R83.
14. Verginadis II, Kanade R, Bell B, et al. A novel mouse model to study image-guided, radiation-induced intestinal injury and preclinical screening of radioprotectors. *Cancer Res* 2017;77:908-917.
15. Tarazi M, Jamel S, Mullish BH, Markar SR, Hanna GB. Impact of gastrointestinal surgery upon the gut microbiome: A systematic review. *Surgery* 2022;171:1331-1340.
16. Donaldson GP, Lee SM, Mazmanian SK. Gut biogeography of the bacterial microbiota. *Nat Rev Microbiol* 2016;14:20-32.
17. Gevers D, Kugathasan S, Denson LA, et al. The treatment-naive microbiome in new-onset Crohn's disease. *Cell Host Microbe* 2014;15:382-392.
18. Leite GGS, Weitsman S, Parodi G, et al. Mapping the segmental microbiomes in the human small bowel in comparison with stool: A REIMAGINE study. *Dig Dis Sci* 2020;65:2595-2604.
19. Bialkowska AB, Ghaleb AM, Nandan MO, Yang VW. Improved swiss-rolling technique for intestinal tissue preparation for immunohistochemical and immunofluorescent analyses. *J Vis Exp* 2016:54161.
20. Rebeck ON, Wallace MJ, Prusa J, et al. A yeast-based oral therapeutic delivers immune checkpoint inhibitors to reduce intestinal tumor burden. *Cell Chem Biol* 2025;32:98-110.e7.
21. Bankhead P, Loughrey MB, Fernández JA, et al. QuPath: Open source software for digital pathology image analysis. *Sci Rep* 2017;7:16878.
22. Callahan BJ, McMurdie PJ, Rosen MJ, et al. DADA2: High-resolution sample inference from Illumina amplicon data. *Nat Methods* 2016;13:581-583.
23. Quast C, Pruesse E, Yilmaz P, et al. The SILVA ribosomal RNA gene database project: Improved data processing and web-based tools. *Nucleic Acids Res* 2013;41:D590-D596.
24. Oksanen J, et al. Package 'vegan'. Community ecology package, version 2, 1-295 (2013).
25. McMurdie PJ, Holmes S. phyloseq: An R package for reproducible interactive analysis and graphics of microbiome census data. *PloS One* 2013;8:e61217.
26. Schliep KP. phangorn: Phylogenetic analysis in R. *Bioinformatics* 2011;27:592-593.
27. Li S, Vogtmann E, Graubard BI, et al. fast.adonis: A computationally efficient non-parametric multivariate analysis of microbiome data for large-scale studies. *Bioinform Adv* 2022;2:vbac044.
28. pairwiseAdonis2: Pairwise multilevel comparison using adonis2 v. 0.4.1 (2020).
29. Mallick H, Rahnavard A, McIver LJ, et al. Multivariable association discovery in population-scale meta-omics studies. *PLoS Comput Biol* 2021;17:e1009442.
30. Gross S, Gammon ST, Moss BL, et al. Bioluminescence imaging of myeloperoxidase activity in vivo. *Nat Med* 2009;15:455-461.
31. Velalopoulou A, Karagounis IV, Cramer GM, et al. FLASH proton radiotherapy spares normal epithelial and mesenchymal tissues while preserving sarcoma response. *Cancer Res* 2021;81:4808-4821.
32. Weiber S, Bjelkengren G, Rank F, Jiborn H, Zederfeldt B. Radiation effects in the colon. An experimental study in the rat. *Acta Oncol* 1993;32:565-569.
33. Bell BI, Koduri S, Salas Salinas C, et al. Interleukin 6 signaling blockade exacerbates acute and late injury from focal intestinal irradiation. *Int J Radiat Oncol Biol Phys* 2019;103:719-727.
34. Rübe CE, Grudzenski S, Kühne M, et al. DNA double-strand break repair of blood lymphocytes and normal tissues analysed in a preclinical mouse model: Implications for radiosensitivity testing. *Clin Cancer Res* 2008;14:6546-6555.
35. McCarty Jr KS, Miller LS, Cox EB, Konrath J, McCarty Sr KS. Estrogen receptor analyses. Correlation of biochemical and immunohistochemical methods using monoclonal antireceptor antibodies. *Arch Pathol Lab Med* 1985;109:716-721.
36. Anandakumar H, Rauch A, Wimmer MI, et al. Segmental patterning of microbiota and immune cells in the murine intestinal tract. *Gut Microbes* 2024;16:2398126.
37. Kavanagh BD, Pan CC, Dawson LA, et al. Radiation dose-volume effects in the stomach and small bowel. *Int J Radiat Oncol Biol Phys* 2010;76:S101-S107.
38. Yu JB, Sun Y, Jia AY, et al. Increasing use of shorter-course radiotherapy for prostate cancer. *JAMA Oncol* 2023;9:1696-1701.
39. Chang BK, Timmerman RD. Stereotactic body radiation therapy: A comprehensive review. *Am J Clin Oncol* 2007;30:637-644.
40. Gu J, Chen YZ, Zhang ZX, et al. At what dose can total body and whole abdominal irradiation cause lethal intestinal injury among C57BL/6J mice? *Dose Response* 2020;18:1559325820956783.
41. Chang DT, Schellenberg D, Shen J, et al. Stereotactic radiotherapy for unresectable adenocarcinoma of the pancreas. *Cancer* 2009;115:665-672.
42. Casteleyn C, Rekecki A, Van der Aa A, Simoens P, Van den Broeck W. Surface area assessment of the murine intestinal tract as a prerequisite for oral dose translation from mouse to man. *Lab Anim* 2010;44:176-183.
43. Osborne JW, Prasad KN, Zimmerman GR. Changes in the rat intestine after x-irradiation of exteriorized short segments of ileum. *Radiat Res* 1970;43:131-142.
44. Ferrie S, Webster A, Wu B, Tan C, Carey S. Gastrointestinal surgery and the gut microbiome: A systematic literature review. *Eur J Clin Nutr* 2021;75:12-25.
45. Brunner TB, Haustermans K, Huguet F, et al. ESTRO ACROP guidelines for target volume definition in pancreatic cancer. *Radiother Oncol* 2021;154:60-69.
46. Murphy JD, Christman-Skieller C, Kim J, et al. A dosimetric model of duodenal toxicity after stereotactic body radiotherapy for pancreatic cancer. *Int J Radiat Oncol Biol Phys* 2010;78:1420-1426.
47. Alam A, Leoni G, Quiros M, et al. The microenvironment of injured murine gut elicits a local pro-restitutive microbiota. *Nat Microbiol* 2016;1:15021.
48. He KY, Lei XY, Wu DH, et al. Akkermansia muciniphila protects the intestine from irradiation-induced injury by secretion of propionic acid. *Gut Microbes* 2023;15:2293312.
49. Nagpal S, Srivastava SK. Colon or semicolon: Gut sampling microdevices for omics insights. *NPJ Biofilms Microbiomes* 2024;10:97.
50. Kastl Jr AJ, Terry NA, Wu GD, Albenberg LG. The structure and function of the human small intestinal microbiota: Current understanding and future directions. *Cell Mol Gastroenterol Hepatol* 2020;9:33-45.
51. Booijink CC, El-Aidy S, Rajilić-Stojanović M, et al. High temporal and inter-individual variation detected in the human ileal microbiota. *Environ Microbiol* 2010;12:3213-3227.
52. Russell A, Copio JN, Shi Y, et al. Reduced housing density improves statistical power of murine gut microbiota studies. *Cell Rep* 2022;39:110783.
53. Fröhlich E, Wahl R. Microbiota and thyroid interaction in health and disease. *Trends Endocrinol Metab* 2019;30:479-490.
54. Rausch P, Basic M, Batra A, et al. Analysis of factors contributing to variation in the C57BL/6J fecal microbiota across German animal facilities. *Int J Med Microbiol* 2016;306:343-355.
55. Kohi S, Macgregor-Das A, Dbouk M, et al. Alterations in the duodenal fluid microbiome of patients with pancreatic cancer. *Clin Gastroenterol Hepatol* 2022;20:e196-e227.
56. Kartal E, Schmidt TSB, Molina-Montes E, et al. A faecal microbiota signature with high specificity for pancreatic cancer. *Gut* 2022;71:1359-1372.
57. Nishijima S, Stankevic E, Aasmets O, et al. Fecal microbial load is a major determinant of gut microbiome variation and a confounder for disease associations. *Cell* 2025;188:222-236.e215.
58. Liu F, Lu H, Dong B, et al. Systematic evaluation of the viable microbiome in the human oral and gut samples with spike-in gram+/- bacteria. *mSystems* 2023;8:e0073822.
59. Jing Y, Wang Q, Bai F, et al. Age-related alterations in gut homeostasis are microbiota dependent. *NPJ Biofilms Microbiomes* 2025;11:51.
60. Li H, Kucharavy HC, Hajj C, et al. Radiation-induced gastrointestinal (GI) syndrome as a function of age. *Cell Death Discov* 2023;9:31.
61. Shiao SL, Kershaw KM, Limon JJ, et al. Commensal bacteria and fungi differentially regulate tumor responses to radiation therapy. *Cancer Cell* 2021;39:1202-1213.e6.
62. Nicolatou-Galitis O, Velegraki A, Sotiropoulou-Lontou A, et al. Effect of fluconazole antifungal prophylaxis on oral mucositis in patients with head and neck cancer receiving radiotherapy. *Support Care Cancer* 2006;14:44-51.